Catalysts **2014**, *4*, 129-145; doi:10.3390/catal4020129

OPEN ACCESS

catalysts

ISSN 2073-4344

www.mdpi.com/journal/catalysts

Article

In Situ XANES/XPS Investigation of Doped Manganese Perovskite Catalysts

Daniel Mierwaldt [1], Stephanie Mildner [1], Rosa Arrigo [2], Axel Knop-Gericke [2], Emanuel Franke [1], Andreas Blumenstein [1], Jörg Hoffmann [1] and Christian Jooss [1,*]

[1] Institut für Materialphysik, Georg-August-Universität Göttingen, Friedrich-Hund-Platz 1, 37077 Göttingen, Germany; E-Mails: dmierwaldt@ump.gwdg.de (D.M.); sraabe@ump.gwdg.de (S.M.); efranke@ump.gwdg.de (E.F.); ablumenstein@ump.gwdg.de (A.B.); jhoffmann@ump.gwdg.de (J.H.)

[2] Fritz-Haber-Institut der Max-Planck-Gesellschaft, Faradayweg 4-6, 14195 Berlin, Germany; E-Mails: arrigo@fhi-berlin.mpg.de (R.A.); knop@fhi-berlin.mpg.de (A.K.-G.)

* Author to whom correspondence should be addressed; E-Mail: jooss@ump.gwdg.de; Tel.: +49-551-39-5303; Fax: +49-551-39-5000.

Received: 14 February 2014; in revised form: 26 March 2014 / Accepted: 1 April 2014 / Published: 23 April 2014

Abstract: Studying catalysts *in situ* is of high interest for understanding their surface structure and electronic states in operation. Herein, we present a study of epitaxial manganite perovskite thin films ($Pr_{1-x}Ca_xMnO_3$) active for the oxygen evolution reaction (OER) from electro-catalytic water splitting. X-ray absorption near-edge spectroscopy (XANES) at the Mn L- and O K-edges, as well as X-ray photoemission spectroscopy (XPS) of the O 1s and Ca 2p states have been performed in ultra-high vacuum and in water vapor under positive applied bias at room temperature. It is shown that under the oxidizing conditions of the OER a reduced Mn^{2+} species is generated at the catalyst surface. The Mn valence shift is accompanied by the formation of surface oxygen vacancies. Annealing of the catalysts in O_2 atmosphere at 120 °C restores the virgin surfaces.

Keywords: catalysis; oxygen evolution; manganese perovskite; $Pr_{1-x}Ca_xMnO_3$; XANES; XPS; Mn L-edge; active state; oxygen vacancies; surface valence

---

1. Introduction

The search for new energy storage technologies has sparked interest in electro-catalytic water splitting. Its overall efficiency is limited by the oxygen evolution reaction (OER). This half reaction can currently only be driven at high overpotentials because of limiting high potential steps in the multi-electron transfer reaction, where the formation of one O_2 molecule requires the cooperative transfer of four electrons to the catalyst. To facilitate this multi-electron transfer at low overpotential, a catalyst needs to adjust its acceptor states to the oxidation potentials of all involved intermediates. This ability requires a sufficiently complex atomic and electronic structure. Mn–O compounds represent a promising material class due to the flexible Mn valence [1]. Possible shifts in the Mn valence between 2+ and 4+ during the reaction steps may allow the catalyst to adjust the bonding characteristics between an active Mn site and oxygen intermediates.

At present, theoretical works on the catalytic activity of perovskites (ABO_3) are based on strong approximations, such as a frozen, defect free surface [2,3]. Those consider the bonding strength of the B-site cation to oxygen as a universal descriptor for oxygen evolution activity of perovskites. Systematic experimental studies of oxygen evolution activity of various transition metal oxide perovskites show a trend of activity with occupation of antibonding e_g states of the B-site d subshell [4], *i.e.*, a volcano type relation with maximum activity at an e_g occupation of about one electron per B-cation. However, manganites seem not to follow this dependence. The activity may strongly depend on factors such as pH value influencing the geometric and electronic structure of the catalyst surface [5].

We present the investigation of the surface electronic structure of $Pr_{1-x}Ca_xMnO_3$ ($0 < x_{Ca} < 0.8$) by means of X-ray absorption near-edge spectroscopy (XANES) and X-ray photo-emission spectroscopy (XPS). The heterovalent Ca-doping results in a Mn valence shift with a bulk average value varying from 3.0+ ($x_{Ca} = 0.0$) to 3.8+ ($x_{Ca} = 0.8$). To what extent the average valence $Mn^{(3+x)+}$ is comprised of a mixture of Mn^{3+} and Mn^{4+} species, or formed by an intermediate valence state is controversially discussed in the literature [6,7]. A formation of intermediate Mn valences would be consistent with a more "covalent-like" electron density distribution within the Mn 3d–O 2p conduction band. By studying the thresholds and line shapes of the Mn L- and O K-edges, we give evidence for the presence of an intermediate Mn valence.

The central question addressed in this work is the surface electronic structure including the valence of the Mn surface sites during catalytic activity. In the presence of water vapor the surface valence may differ from the bulk value due to the bonding of various adsorbates and the formation of surface defects such as oxygen vacancies. The presented spectra have either been recorded in ultra-high vacuum (UHV), or in contact with water vapor at the crystalline catalyst surface with an applied positive electric potential, nominally corresponding to OER conditions. It is shown, that upon *in situ* activation of the catalyst surface Mn^{2+} coexists with the mean bulk valence of $Mn^{(3+x)+}$. This is consistent with the reversible formation of surface oxygen vacancies as well as surface hydroxide adsorbates. It is furthermore shown that the virgin surface measured under UHV conditions can be restored by annealing at about 120 °C in 0.1 mbar O_2. The formation of surface oxygen vacancies contradicts the expectations from the oxidizing electro-chemical conditions during oxygen evolution and, thus, sheds light onto possible reaction mechanisms.

2. Results and Discussion

2.1. Doping Dependence of Virgin Samples

Mn L-edge and O K-edge spectra of the virgin samples under UHV conditions are shown in Figure 1. The Mn L-edge is split into two separate multiplets L_3 (at 642 eV) and L_2 (at 653 eV) due to spin-orbit interaction of the Mn $2p_{3/2}$ and $2p_{1/2}$ core states. The complex structure of these edges can be attributed to the Mn 3d states due to the octahedral ligand field including hybridization with O 2p states as well as Coulomb and exchange interactions within the 3d states [8–10]. Compared to simple Mn oxides, further complexity of the L_3 edge is produced by the lower local symmetry due to octahedral tilting in the orthorhombic PCMO phase [11]. Linear superposition (Appendix Figure A1) of the spectra at $x_{Ca} = 0$ and 0.8 resulted in poor agreement with the spectra at intermediate doping of $x_{Ca} = 0.3$ and 0.5, which indicates an intermediate valence state of $Mn^{(3+x)+}$ instead of coexisting Mn^{3+} and Mn^{4+} species [12]. This observation clearly supports the statement of a high covalence of the Mn-O bond.

Figure 1. Normalized (see experimental section) X-ray absorption of virgin samples in UHV. (**a**) The Mn L-edge shows the systematic increase in Mn valence with increasing x_{Ca}; (**b**) Intensity of the pre-edge feature of the O K-edge (530 eV) increases with x_{Ca}.

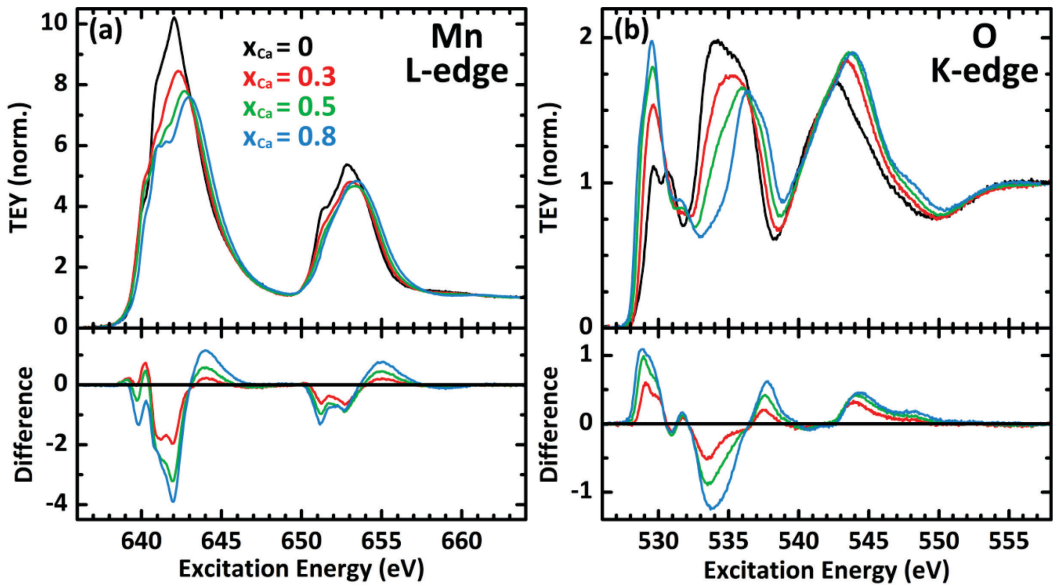

The L_3 peak shifts to higher energies and its area decreases systematically with increasing x_{Ca} and therefore increasing formal Mn valence of $(3 + x_{Ca})+$. A similar trend can be seen for the L_2 edge. This chemical shift is in good agreement with reported results on various manganite perovskites [13,14] and other Mn compounds [9]. According to studies of Mn oxide compounds by means of Electron Energy Loss Spectroscopy (EELS) [15] the decreasing energetic distance ΔE_L between the maxima of the Mn L_2 and L_3 edges (Figure 1a and Table 1) due to increasing x_{Ca} corresponds to an increase in Mn valence. Despite the systematic error resulting from only taking into account the maximum position of the complex L_3 edge structure, our data represent a systematic valence shift as expected from sample stoichiometry (formal bulk valence from 3.0+ to 3.8+). Moreover, the integral intensity ratio of the L_3 and L_2 edges decreases systematically with increasing x_{Ca} (Table 1, for details see Appendix).

According to Riedl *et al.* [16] our data quantitatively represent the expectation of a systematic Mn valence increase between 3+ and 4+.

Table 1. Mn valence indicators obtained from the Mn L- and O K-edge spectra of virgin samples under ultra-high vacuum (UHV) conditions. The energetic distance between the Mn L_3 and L_2 edges (ΔE_L), their intensity ratio (I_3/I_2) after subtraction of a constant L_2 background (BG1) or linear backgrounds for each edge (BG2, see Appendix) as well as the distance between the pre-edge feature and the first main resonance of the O K-edge (ΔE_K) are summarized.

x_{Ca}	formal bulk valence	ΔE_L (eV)	I_3/I_2 (BG1)	I_3/I_2 (BG2)	ΔE_K (eV)
0	3.0+	10.8	2.89	2.54	3.8
0.3	3.3+	10.8	2.88	2.53	5.8
0.5	3.5+	10.6	2.85	2.46	6.3
0.8	3.8+	10.4	2.75	2.32	6.8

The pre-edge region of the O K-edge at roughly 530 eV (Figure 1b) represents excitation into hybridized states containing O 2p and Mn 3d states [17,18]. It is thus a direct expression of the degree of covalence of the Mn–O bond near the Fermi level. Our results show splitting of the pre-edge feature for the undoped $PrMnO_3$ (formal Mn valence of 3+), which can be explained by ligand field interaction and high-spin Hund's coupling resulting in O 2p states hybridized with majority spin Mn e_g states at 529.6 eV and with minority spin Mn t_{2g} states at 530.8 eV [19]. Heterovalent Ca-doping leads to a decreased Mn 3d occupation, which is reflected by the systematic intensity increase at the low energy flank of the pre-edge region. Furthermore, the first main resonance, which results from excitation into hybridized states containing Pr 5d and Ca 3d contributions [20], shifts from 534 eV (x_{Ca} = 0) to 536.4 eV (x_{Ca} = 0.8), which is in good agreement with data reported on various Sr- and Ca-doped rare-earth manganites [11,13]. These trends can be expressed as an increasing energetic distance ΔE_K between the pre-edge feature and the first main resonance (Table 1), which reflects the effects of the hole doping [16].

2.2. In Situ Investigation

In previous work, oxygen evolution at $Pr_{1-x}Ca_xMnO_3$ has been detected in two electrode configurations at sample bias above +1.6 V. These experiments have been performed in liquid water by differential electrochemical mass spectrometry (DEMS) and by mass spectrometry in environmental transmission electron microscopy (ETEM) in water vapor [5]. We here present *in situ* studies of the same catalyst in 0.1 mbar H_2O at sample bias of +2.5 V, where oxygen evolution is expected.

Figure 2 presents the change of the Mn L-edge during catalyst activation. In contact with the water vapor an increase in L_3 and L_2 intensity was observed. To analyze the changes in the Mn valence states, the difference spectra between the UHV virgin spectra and the spectra in water vapor at positive bias have been generated and are shown as filled green curves. With peaks at 640.2, 641.6, and 643.9 eV, they bear a resemblance to a pure Mn^{2+} spectrum, as will be shown in the following section. After heating the samples for 10 min to about 120 °C in 0.1 mbar O_2 the post reaction analysis was done

under UHV conditions. For x_{Ca} = 0.3 and 0.5 the original surface oxidation state was entirely restored, while minor changes remain for x_{Ca} = 0 and 0.8 (filled blue curves).

Figure 2. Normalized Mn L-edge spectra (Total Electron Yield) before (red) and during insertion of 0.1 mbar H_2O with sample bias of +2.5 V against chamber ground (green), as well as in UHV after reoxidation in 0.1 mbar O_2 (blue). Samples with x_{Ca} = 0 (**a**), x_{Ca} = 0.3 (**b**), x_{Ca} = 0.5 (**c**), and x_{Ca} = 0.8 (**d**). Filled curves represent the change from virgin to activated (green) and from virgin to post reaction (blue).

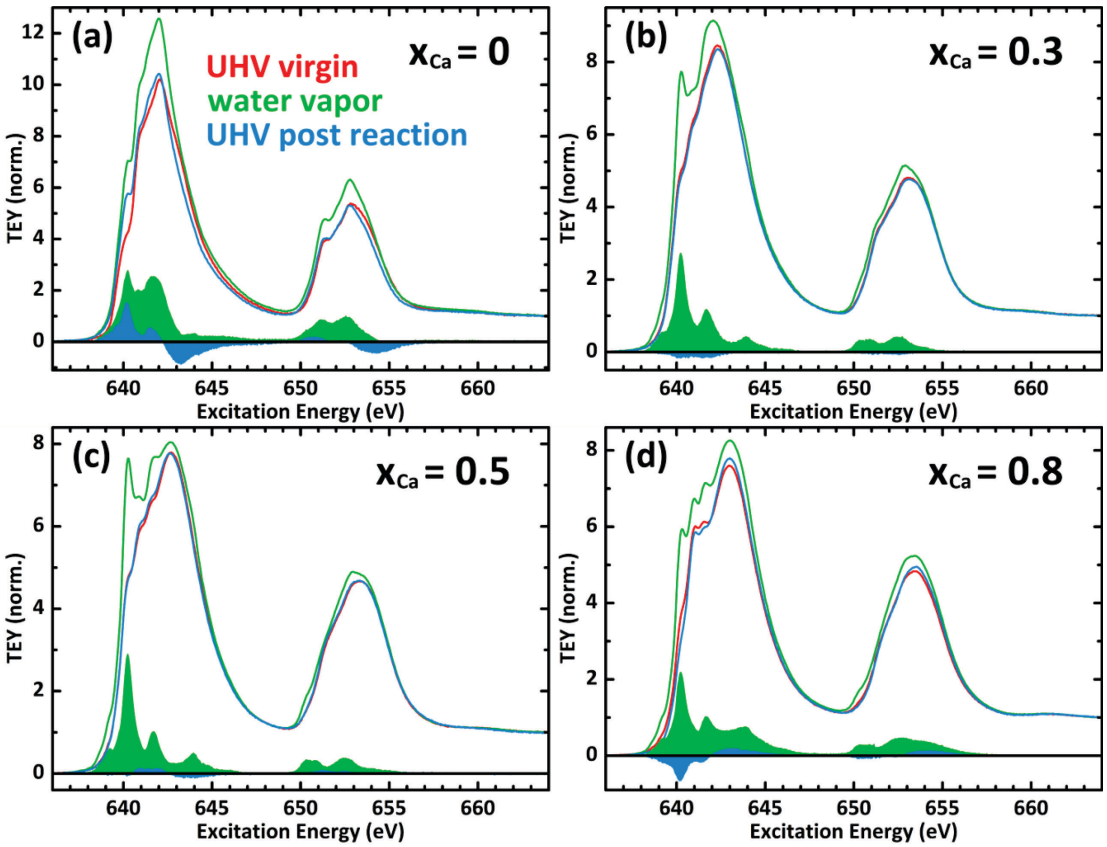

In order to get insight into the changes of the catalyst surface upon contact with liquid water with respect to the effects of water vapor, we compare in Figure 3 the Mn L-edges of a virgin sample at x_{Ca} = 0.8 with a sample which has been pretreated in liquid water without bias application. After keeping the sample in distilled water at room temperature for 60 min, it was directly dried and transferred into the UHV chamber. The pretreatment results in formation of some Mn^{2+} species in addition to the bulk $Mn^{3.8+}$. We observe a slight general decrease of the intensity to background ratio, which may be due to surface adsorbates such as hydroxides.

This pretreated sample has then been investigated by the same *in situ* procedure as the virgin samples, which is shown in Figure 3b. The arising Mn^{2+} spectrum in response to water vapor under positive bias is more pronounced than the one of the virgin sample (Figure 2d), with its two main peaks at 640.2 and 641.6 eV dominating the L_3 edge. After heating the sample for 10 min in 0.1 mbar O_2 and returning to UHV the post reaction analysis shows the recovery of the pretreated state.

Figure 3. Normalized Mn L-edge of pretreated sample (x_{Ca} = 0.8). (**a**) Comparison to virgin sample with x_{Ca} = 0.8 in UHV; (**b**) Pretreated state in UHV (red), in 0.1 mbar H_2O at a bias of +2.5 V against chamber ground (green), and post reaction in UHV (blue).

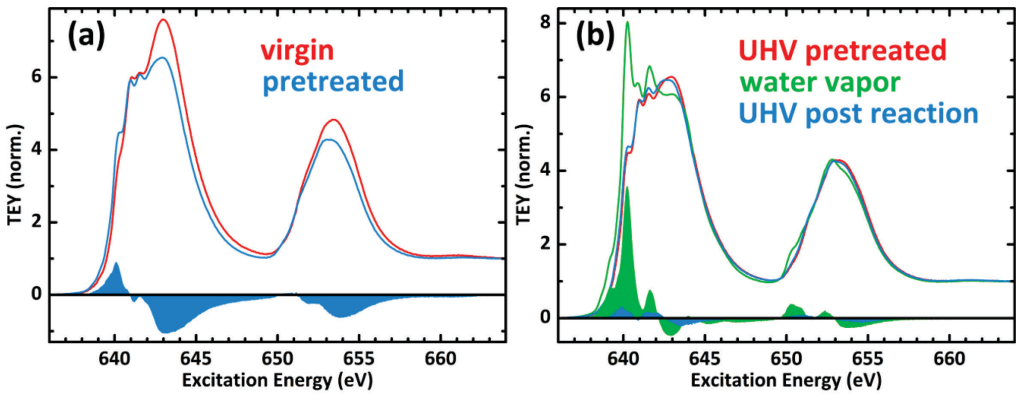

2.3. Mn Surface Species

Except for a small additional feature at 639 eV, the difference spectra of the Mn L_3 edge between virgin and activated state (filled green curves in Figure 2) correspond to a pure Mn^{2+} spectrum (Figure 4), showing good agreement with calculated spectra based on atomic multiplet theory in a cubic crystal field [8] as well as with spectra measured at Mn(II)O_x nanoparticles [21], commercial Mn(II)SO_4 [9], Mn(II)CO_3 [22,23], Mn(II)O [24], and complex Mn(II) compounds [25].

Figure 4. Difference spectra at Mn L-edge between *in situ* activated and virgin state compared with Mn^{2+} spectrum taken from Mette *et al.* [21].

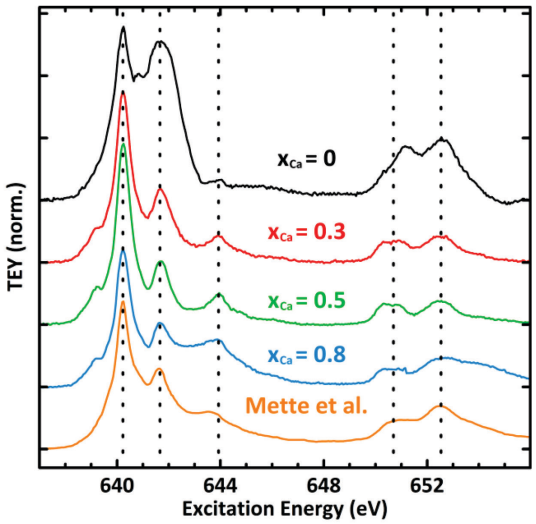

The information depth of XANES TEY spectra is determined by the escape depth of the photoelectrons, which are composed of electrons of quite different energies, namely primary photoelectrons, Auger electrons and secondary electrons. Contributions of the different types of emitted electrons depend on the material, the photon energy and the electron energy dependent transmission function of the detector. Exact values are presently not known. According to a study by Frazer *et al.* [26] on the escape depth of electrons through a Cr layer (Z_{Cr} = 24 compares to

the average Z = 21.5 of $PrMnO_3$) we expect that 50% of the signal originates from the topmost 0.6 nm (O K-edge) and 0.7 nm (Mn L-edge) and 99.9% from the first 6 nm (O K-edge) and 7 nm (Mn L-edge), respectively.

The high reversibility after removing the water vapor by heating samples in oxygen and the nm range information depth of the TEY spectra suggest that the formation of Mn^{2+} species results from surface and/or subsurface O vacancy formation during oxygen evolution [23]. At first sight this fundamentally contradicts the expectations from a "frozen surface—No surface defects" picture, since the Mn valence should increase under the nominally oxidizing conditions with an applied sample bias of +2.5 V *vs.* the grounded chamber. Under such conditions, no overall reduction via pure vacancy formation should take place in the catalyst. Our observations thus indicate that surface oxygen vacancies are directly involved in the reaction mechanism during water oxidation. In such a scenario, the (sub)surface oxygen may represent an exchange site for oxygen based intermediates, which is affected by the state of neighboring Mn sites. Alternatively, a Mn valence decrease may be induced by surface adsorbates such as OH^- and OOH^-, which exhibit a lower formal valence compared to O^{2-}. However, the integral L_3 intensity increase due to Mn^{2+} formation of 8.5% to 13.9% is quite strong considering the information depth of the order of several nm. We therefore conclude that the changes are not mainly due to surface adsorbates, but rather to formation of surface-near oxygen vacancies. The corresponding redox process is visible in cyclic voltammetry as a reversible surface process centered at $U_0 \approx +1$ V *vs.* SHE (see experimental section). It can be interpreted according to:

$$2\ Pr^{3+}_{1-x}Ca^{2+}_{x}Mn^{(3-x)+}O^{2-}_{3} + 2\ e^- \Leftrightarrow 2\ Pr^{3+}_{1-x}Ca^{2+}_{x}Mn^{(3+x)+}_{1-y}Mn^{2+}_{y}O^{2-}_{2.5} + V''_O + \tfrac{1}{2}\ O_2. \quad (1)$$

Although the chemical equilibrium at reduced oxygen partial pressure is generally shifted towards oxygen vacancy formation, our finding that reoxidation by healing of vacancies can take place at a similar partial pressure (0.1 mbar O_2) as their formation seems to exclude this effect as the main driving force. We rather assume that surface oxygen formation is a non-equilibrium property of the active catalyst during OER.

This assumption is supported by the observed doping dependence of the Mn^{2+} formation. Our *in situ* results show that the accordance of the differential spectra with the pure Mn^{2+} reference is best for intermediate doping of x_{Ca} = 0.3 and 0.5, while only minor deviations are observed for x_{Ca} = 0.8, namely an increased intensity around the 644 eV peak of the L_3 edge and at the high energy tail of the L_2 edge (Figure 4). Additionally, the changes of integral intensity (from 630 to 665 eV) due to Mn^{2+} formation are relatively small for x_{Ca} = 0.3 (+8.7%) and 0.5 (+8.5%) compared to the values at x_{Ca} = 0 (+13.9%) and 0.8 (+10.6%) (Figure 2). Finally, samples at x_{Ca} = 0.3 and 0.5 show a higher reversibility in UHV post reaction analysis. These findings thus indicate a higher (electro) chemical stability at intermediate x_{Ca}, which is in contrast to the monotonic decrease of the formation energy of manganite perovskites from the metal elements and O_2 with increasing Ca-doping [2]. The hereby observed maximum stability at intermediate x_{Ca} is in good agreement with environmental transmission electron microscopy results comparing low/intermediate x_{Ca} to high Ca-doping [5], as well as stability analysis in the whole doping range by *ex situ* cyclic voltammetry (see supplementary information in [5]).

In contrast to oxygen evolution in water vapor, the pretreatment of the catalyst in liquid water may facilitate the formation of an A-cation deficient surface layer, *i.e.*, the irreversible dissolution of Ca^{2+}. Evidence for the irreversibility of the pretreatment is given by post reaction reoxidation in O_2

atmosphere, which results in restoration of the pretreated instead of the virgin state (Figure 3b, blue curve). In addition to Ca^{2+} dissolution, formation of O vacancies and interstitial hydrogen can take place to some extent in the absence of external bias. Our data, thus, suggest that these processes overcompensate the effect of the oxidative Ca^{2+} dissolution. We cannot entirely exclude that also diffusion of vacancies or hydrogen into deeper subsurface regions during liquid water exposure contribute to the changes in the pretreated sample.

2.4. XPS

Due to *in situ* activation in water vapor intense additional peaks emerge in the X-ray photoelectron spectra of the Ca $2p_{3/2}$ and Ca $2p_{1/2}$ states respectively (347.5 and 351 eV), as well as of the O 1s states (532 eV) shown for the sample at x_{Ca} = 0.5 in Figure 5a and b. According to studies on $La_{0.6}Ca_{0.4}CoO_3$ [27,28], the changed structure of the Ca 2p spectra is consistent with the formation of surficial $Ca(OH)_2$ and CaO species. The broad additional O 1s peak indicates the formation of various weakly bound O^- species on the surface including hydroxide adsorbates and point defects in the perovskite lattice. This has been found by studies on $La_{1-x}Sr_xMnO_3$ [29], $La_{0.6}Ca_{0.4}CoO_3$ [27], $La_{1-x}Ce_xMnO_3$ [30], $La_{1-x}Ca_xMnO_3$ [31], $CaO/Ca(OH)_2$ [32] and $LaMO_3$ (M = Rh, Ni, Co, Fe, Mn, Cr) [33]. For a more detailed peak analysis see Appendix.

Figure 5. X-ray photoemission spectra of a PCMO film with x_{Ca} = 0.5. (**a**) Ca 2p states before (red) and during insertion of 0.1 mbar H_2O with sample bias of +2.5 V against chamber ground (green), as well as in UHV after reoxidation in 0.1 mbar O_2 (blue); (**b**) O 1s states; (**c**) Depth profiling of Ca 2p states in active catalyst, ranging from 1 nm (E_{exc} = 568 eV) to 1.5 nm (E_{exc} = 1168 eV); (**d**) Depth profiling of O 1s states with the same information depths.

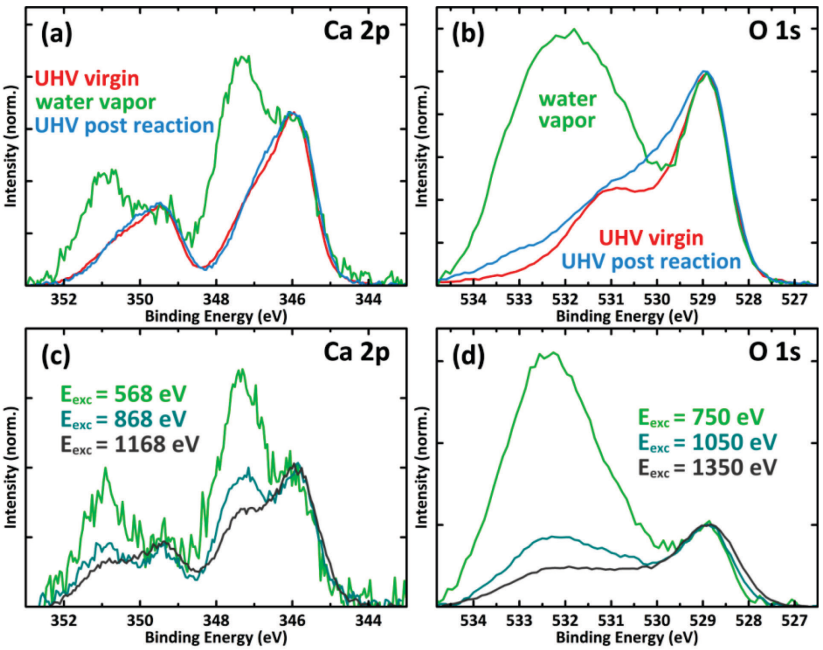

The spectra presented in Figure 5a,b have been recorded at photon energies of 568 and 750 eV respectively, resulting in kinetic energies of the photoelectrons of about 220 eV. This corresponds to

an information depth of roughly 1 nm [34]. To investigate the nature of the additional Ca and O species due to *in situ* activation the excitation energies were increased by 300 and 600 eV. Increasing the kinetic energy of the photoelectrons to 820 eV results in an information depth of about 1.5 nm. The decreasing intensity of the active species with increasing photon energy (Figure 5c,d), thus, indicates near surface changes.

3. Experimental Section

3.1. Sample Preparation and Characterization

$Pr_{1-x}Ca_xMnO_3$ (PCMO) thin films at doping levels of x_{Ca} = 0, 0.3, 0.5 and 0.8 have been deposited by reactive ion beam sputtering from stoichiometric targets. The Xe working gas partial pressure amounted to 1×10^{-4} mbar and the O_2 partial pressure was 1.4×10^{-4} mbar. The films have a thickness of about 300 nm and have been deposited on 200 nm Pt layers, which provide the electric back contact. These Pt films have previously been deposited on commercial MgO (001) single crystal substrates.

Figure 6. XRD scans in θ–2θ geometry. The intense substrate peaks correspond to Pt (111) and MgO (001). $PrMnO_3$ (black) exhibits a (001)/(110) twin structure, while samples with x_{Ca} = 0.3 (red) and 0.5 (green), as well as the two samples with x_{Ca} = 0.8 (blue and cyan) show a (100)/(010)/(112) texture.

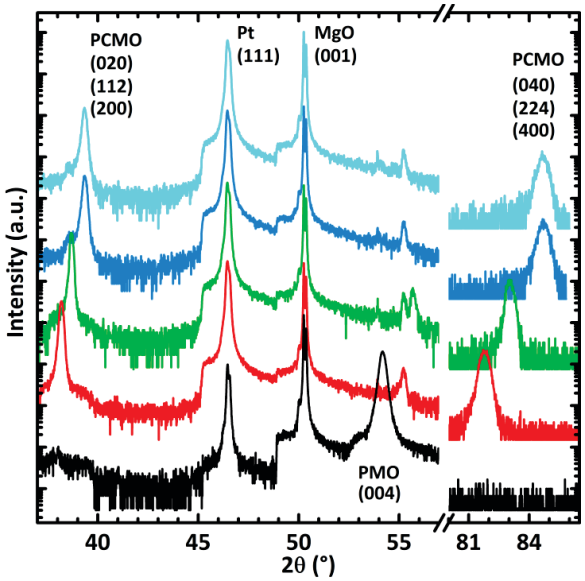

The films have been characterized by means of X-ray diffraction (XRD) in θ–2θ geometry using an X'Pert MRD diffractometer (Philips B.V., Almelo, Netherlands) with Co K_α radiation from a tube operated at 40 kV and 30 mA. Figure 6 summarizes the XRD results of the five investigated samples. Note that the spectra of two different samples at x_{Ca} = 0.8 are shown in Figure 6; the sample shown in cyan was used for pretreatment in liquid water. The two intense peaks at 46.5° and 50.3° can be attributed to the Pt (111) layer and the MgO (001) substrate respectively. The $PrMnO_3$ film (black curve) shows a (001) orientation with (110) twins, represented by the broadened peak at 54.2°. The Ca-doped samples (colored curves) exhibit two peaks at 38.2°–39.4° and 81.8°–84.7° respectively, revealing a texture containing (100), (010), and (112) orientations, which cannot be further

distinguished due to overlap of the (200), (020) and (112) peaks. The systematic shift of these two peaks to higher angles with increasing x_{Ca} represents the reduction in lattice parameter due to different octahedral tilts and Mn–O bonding length [35]. For the sample with x_{Ca} = 0.5 (green curve) (001) misorientations (<33 vol-%) are observed, represented by the (004) peak at 55.7°. Additional small peaks from 53° to 56° result from artifacts due to other X-ray wavelengths.

The surface morphology has been investigated by scanning electron microscopy (SEM) using a LEO Supra 35 (Carl Zeiss NTS GmbH, Oberkochen, Germany). A representative SEM image for each doping level x_{Ca} is shown in Figure 7, revealing compact films. The sample with x_{Ca} = 0 exhibits a rod-like surface morphology due to the (110) twins (Figure 7a), while the samples with x_{Ca} = 0.3 and 0.5 show a plate-like morphology (Figure 7b,c) which most probably corresponds to the [100]/[010] orientations. The sample with x_{Ca} = 0.8 shows a morphology of higher complexity which may indicate a non-unique in-plane epitaxy (Figure 7d). Additionally, it is revealed that the sample surfaces with x_{Ca} = 0.3 and 0.5 contain MnO_x precipitates, which however cover only <2% of the surface.

Figure 7. SEM images of samples with x_{Ca} = 0 (**a**), 0.3 (**b**), 0.5 (**c**), and 0.8 (**d**) after XANES/XPS investigation. Shown is the secondary electron contrast.

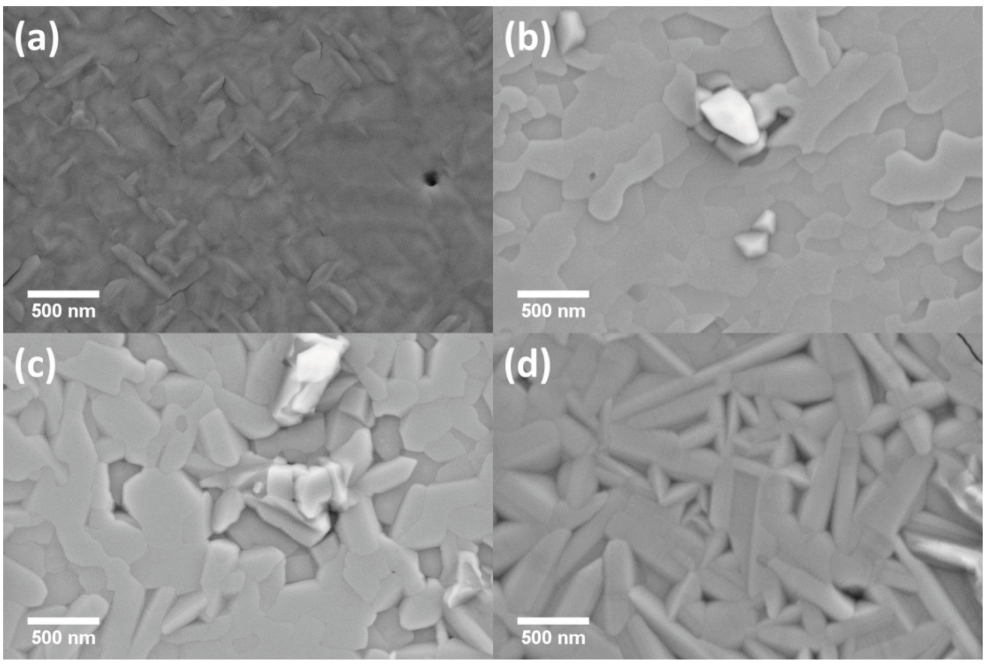

The catalytic activity for oxygen evolution from water splitting has been investigated at comparable samples with x_{Ca} = 0.3 by cyclic voltammetry (CV). Figure 8 shows CV curves measured at a PCMO thin film at sweep rates of 2.5, 5, and 10 mV/s. A Pt counter electrode and commercial Ag/AgCl reference electrode have been used in aqueous 0.1 m Na_2SO_4 (pH 7). In addition to oxygen evolution above +1.2 V *vs.* SHE a reversible surface redox process is observed, which is centered at $E_0 \approx +1$ V *vs.* SHE. A more detailed CV investigation of different PCMO stoichiometries has been published elsewhere [5], where this process has been interpreted as oxygen vacancy formation according to Equation (1). No changes in surface morphology have been observed by post reaction SEM investigation.

Figure 8. CV curves of a PCMO sample with x_{Ca} = 0.3 showing oxygen evolution above +1.2 V *vs.* SHE and a reversible redox process centered at +1.0 V *vs.* SHE (pH 7).

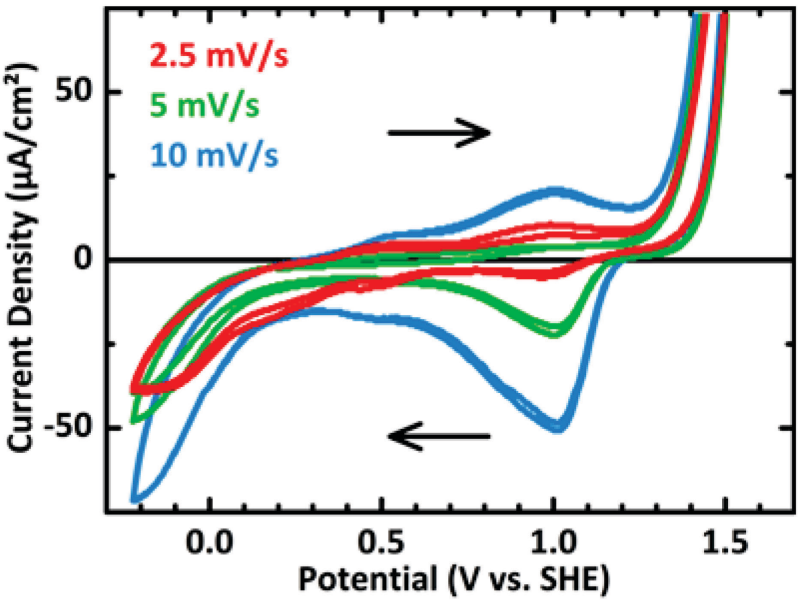

3.2. In Situ XANES/XPS Measurements

X-ray absorption near edge spectroscopy (XANES) as well as X-ray photo-emission spectroscopy (XPS) of various edges and states has been performed at the BESSY II synchrotron facility of the Helmholtz-Zentrum Berlin, Germany (HZB), using the near ambient-pressure XPS endstation of the Fritz-Haber-Institut of the Max-Planck-Gesellschaft (FHI-MPG) at the ISISS beamline. The instrumental setup by Knop-Gericke and co-workers is described in detail elsewhere [36].

For XANES at the Mn L-edge the excitation energy was swept from 630 to 665 eV, while the O K-edge was measured from 520 to 565 eV. The scan rate was 0.5 eV/s in continuous driving mode of the plane-grating monochromator. The fixed-focus constant was set to c_{ff} = 2.25 and the exit slit to 60 μm [37]. The presented spectra have been measured in total electron yield mode (TEY). Energy shifts have been corrected on the basis of the simultaneously measured characteristic absorption spectrum of a focusing mirror. Intensities have been normalized with respect to impinging photon flux. A linear background was subtracted and the spectra were intensity normalized to unity at 664 eV for the Mn L-edge and at 558 eV for the O K-edge to account for the increased signal in water vapor due to inelastic scattering of photoelectrons with gas molecules.

For collecting the photoemission spectra the monochromator was set to c_{ff} = 2.25 with an exit slit of 111 μm. Emission from the Ca 2p states has been recorded at an excitation energy of 568 eV, while emission from the O 1s states has been recorded at an excitation energy of 750 eV. For depth profiling each of the excitation energies was increased by 300 and 600 eV respectively. The step size was 50 meV for Ca 2p and 100 meV for O 1s spectra. All spectra were collected using a pass energy of 20 eV and a dwell time of 100 ms. Spectra have been intensity normalized with respect to impinging photon flux. A linear as well as a Shirley-type background were subtracted [38]. To account for loss of total signal intensity during water vapor exposure compared to UHV measurements due to inelastic scattering of photoelectrons at gas molecules, the spectra were then normalized with respect to the

intensity of the bulk-like peaks of the Ca $2p_{3/2}$ states at 346 eV or the O 1s states at 529 eV respectively. These bulk-like peaks have also been used for energy alignment, e.g., for subtraction of sample bias.

Experiments have been conducted in ultra-high vacuum (UHV) and in 0.1 mbar H_2O vapor with an applied sample bias of +2.5 V between the sample back contact and the chamber (ground). All measurements have been performed at room temperature. Before returning to UHV conditions the samples were heated to approximately 120 °C for 10 min and cooled for another 10 min in 0.1 mbar O_2 to remove accumulated surface carbon and to reestablish a fully oxygenized sample surface.

4. Conclusions

$Pr_{1-x}Ca_xMnO_3$ thin films in the doping range between $x_{Ca} = 0$ and 0.8 have been studied with respect to electro-catalytic oxygen evolution. It is found that the doping dependent Mn valence cannot be described by a mixture of Mn^{3+} and Mn^{4+} species but rather by an intermediate $Mn^{(3+x)+}$ state. This finding corroborates the picture of covalent-like contributions to the charge distribution in the antibonding Mn 3d e_g–O 2p states, which are relevant for electron transfer from oxygen-based species to Mn sites during water oxidation. *In situ* studies under nominally oxidizing conditions for oxygen evolution reveal the coexistence of a Mn^{2+} surface species with the bulk Mn valence state. It is shown that the surface activation involves the reversible formation of surface oxygen vacancies. The observed changes are fully reversible with respect to annealing in O_2 atmosphere at 120 °C.

We conclude that the Mn valence shift is mainly due to surface oxygen vacancy formation, which are formed by the reaction steps during water oxidation despite of the nominally oxidizing conditions. We propose that such oxygen vacancies are part of the active catalyst structure and are involved as a docking site for water molecules and reaction intermediates.

Since the occupation of antibonding e_g states is changed in operation, the application of a rigid molecular orbital filling model to describe catalytic activity as a function of bulk bonding strength seems to be very limited. The bulk occupation of these states, which can be controlled by heterovalent doping, can be strongly modified at the activated surface.

Acknowledgments

The Helmholtz-Zentrum Berlin (HZB) is acknowledged for the allocation of synchrotron measurement time. We are grateful to Helge Stein who supported the XANES and XPS measurements. Financial support by the Deutsche Forschungsgemeinschaft through the CRC 1073 project C02 is gratefully acknowledged. We thank Robert Schlögl for fruitful discussions.

Conflicts of Interest

The authors declare no conflict of interest.

Appendix

A1. Linear Superposition of Experimental Mn L-Edges

To deal with the question whether the average Mn valence is comprised of a mixture of Mn^{3+} and Mn^{4+} species or formed by an intermediate valence state of $Mn^{(3+x)+}$, we compared stoichiometric linear superposition of Mn L-edges at high and low x_{Ca} to measured spectra at intermediate x_{Ca}. As shown in Figure A1, the stoichiometric superpositions (blue curves) show significant systematic deviations from the corresponding measurements. Variations can be compared by the difference spectra which are shown as filled blue curves. They exhibit a minimum at 640.2 eV as well as two maxima at 641.0 and 642.0 eV respectively. According to Kanamori *et al.* [12] the bad compliance indicates an intermediate valence state instead of coexisting species. This result indicates significant covalent contributions to the Mn-O bond, *i.e.*, a charge density distribution at the upper valence band edge which is more or less centered at the Mn–O bond instead of forming Mn^{3+}/Mn^{4+} species.

Figure A1. Comparison of linear superpostition of Mn L-edges at high and low x_{Ca} to spectra at intermediate x_{Ca}. The superpositions (blue) are assembled according to the expected nominal concentrations of the Mn^{3+} and Mn^{4+} species as indicated by the formulas in blue color.

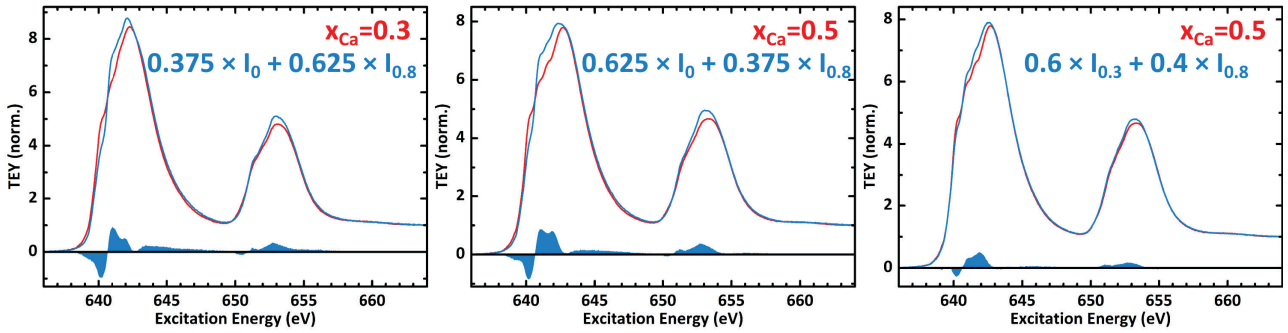

A2. Intensity Ratio of the Mn $L_{3,2}$-Edges

For Electron Energy Loss Spectroscopy (EELS) in transmission electron microscopy (TEM) of white lines like the Mn L-edge a Hartree-Slater-type background model has been established [15]. Since the physical processes in TEY-XANES experiments are quite different, we used a constant as well as a linear background model for quantification of the integral Mn $L_{3,2}$ edge intensities of the virgin samples. The backgrounds are illustrated in Figure A2. A constant L_2 background (BG1) was used from 649.3 to 658.0 eV, while two linear backgrounds (BG2) were used from 637.3 to 649.3 eV and from 649.3 to 658.0 eV respectively.

Figure A2. Simple background models used for quantification of Mn $L_{3,2}$ intensities.

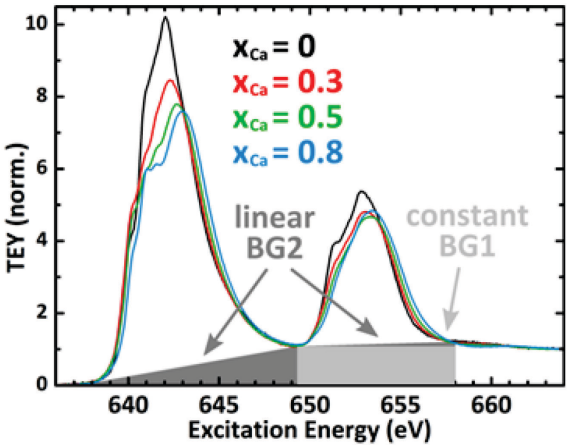

A3. XPS

Spin-orbit interaction splits the Ca 2p states into $2p_{1/2}$ and $2p_{3/2}$ substates at binding energies of roughly 350 and 346 eV respectively. The structure of the virgin perovskite lattice at x_{Ca} = 0.5 shown in Figure A3a reveals further splitting into a total of four peaks labeled P_1 and P_2 for the $2p_{3/2}$ as well as P_3 and P_4 for the $2p_{1/2}$ states. P_2 and P_4 represent surface sites exhibiting less chemical shift compared to the P_1 and P_3 subsurface sites. Upon *in situ* activation in 0.1 mbar water vapor at a sample bias of +2.5 V against the grounded chamber our data show the emergence of a second Ca species represented by the peaks labeled A_1 and A_2. According to studies on $La_{0.6}Ca_{0.4}CoO_3$ [27,28] this could correspond to formation of surficial $Ca(OH)_2$ and CaO. Reoxidation in 0.1 mbar O_2 fully restores the virgin state of the surface (blue curves in Figure A3a).

The four peaks of the O 1s states are shown in Figure A3b. The O^{2-} species of the perovskite lattice is represented by peak P_1 (subsurface) and P_2 (surface). P_3 corresponds to various weakly bound O^- and OH^- surface species, while P_4 represents adsorbed H_2O molecules. Upon in situ activation P_3 and P_4 increase significantly. Reoxidation of the sample leaves a slightly increased intensity of P_2 and P_4 compared to the virgin surface.

Figure A3. Peak analysis of XPS data before (red) and during insertion of 0.1 mbar H_2O with sample bias of +2.5 V against grounded chamber (green), as well as in UHV after reoxidation in 0.1 mbar O2 (blue). (**a**) Ca 2p states; (**b**) O 1s states.

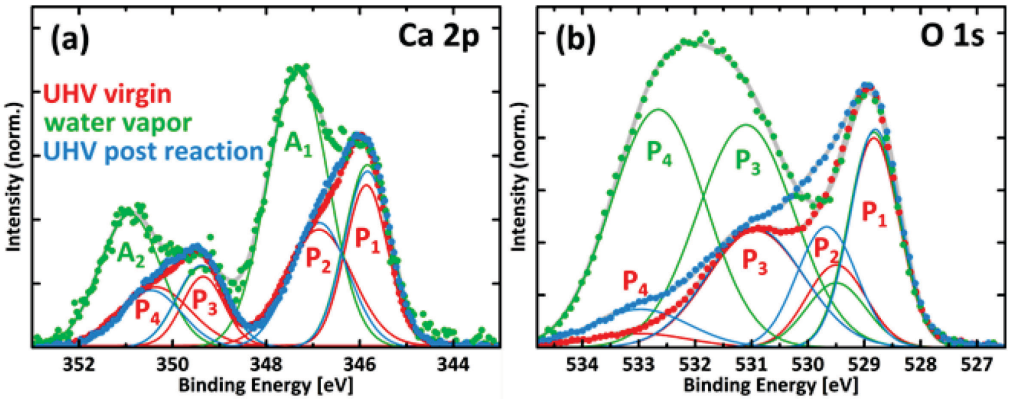

References

1. Armstrong, F.A. Why did nature choose manganese to make oxygen? *Philos. T. Roy. Soc. B* **2008**, *363*, 1263–1270.
2. Calle-Vallejo, F.; Martínez, J.I.; García-Lastra, J.M.; Mogensen, M.; Rossmeisl, J. Trends in Stability of Perovskite Oxides. *Angew. Chem. Int. Ed.* **2010**, *49*, 7699–7701.
3. Man, I.C.; Su, H.-Y.; Calle-Vallejo, F.; Hansen, H.A.; Martínez, J.I.; Inoglu, N.G.; Kitchin, J.; Jaramillo, T.F.; Nørskov, J.K.; Rossmeisl, J. Universality in Oxygen Evolution Electrocatalysis on Oxide Surfaces. *ChemCatChem* **2011**, *3*, 1159–1165.
4. Suntivich, J.; May, K.J.; Gasteiger, H.A.; Goodenough, J.B.; Shao-Horn, Y. A Perovskite Oxide Optimized for Oxygen Evolution Catalysis from Molecular Orbital Principles. *Science* **2011**, *334*, 1383–1385.
5. Raabe, S.; Mierwaldt, D.; Ciston, J.; Uijttewaal, M.; Stein, H.; Hoffmann, J.; Zhu, Y.; Blöchl, P.; Jooss, C. *In Situ* Electrochemical Electron Microscopy Study of Oxygen Evolution Activity of Doped Manganite Perovskites. *Adv. Funct. Mater.* **2012**, *22*, 3378–3388.
6. Raveau, B. The crucial role of mixed valence in the magnetoresistance properties of manganites and cobaltites. *Philos. T. Roy. Soc. A* **2008**, *366*, 83–92.
7. Grenier, S.; Hill, J.P.; Gibbs, D.; Thomas, K.J.; von Zimmermann, M.; Nelson, C.S.; Kiryukhin, V.; Tokura, Y.; Tomioka, Y.; Casa, D.; *et al.* Resonant X-ray diffraction of the magnetoresistant perovskite $Pr_{0.6}Ca_{0.4}MnO_3$. *Phys. Rev. B* **2004**, *69*, 134419.
8. De Groot, F.M.F.; Fuggle, J.C.; Thole, B.T.; Sawatzky, G.A. 2p X-ray absorption of 3d transition-metal compounds: An atomic multiplet description including the crystal field. *Phys. Rev. B* **1990**, *42*, 5459–5468.
9. Grush, M.M.; Chen, J.; Stemmler, T.L.; George, S.J.; Ralston, C.Y.; Stibrany, R.T.; Gelasco, A.; Christou, G.; Gorun, S.M.; Penner-Hahn, J.E.; *et al.* Manganese L-Edge X-ray Absorption Spectroscopy of Manganese Catalase from Lactobacillus plantarum and Mixed Valence Manganese Complexes. *J. Am. Chem. Soc.* **1996**, *118*, 65–69.
10. Imada, S.; Suga, S.; Muro, T.; Ueda, S.; Jung, R.-J.; Kotsugi, M.; Saitoh, Y.; Matsushita, T.; Kuwahara, H.; Moritomo, H.; *et al.* Local magnetic states in $La_{1-x}Sr_xMnO_3$ and $Nd_{1-x}Sr_xMnO_3$. *Physica B* **2000**, *281–282*, 498–499.
11. Subías, G.; García, J.; Sánchez, M.C.; Blasco, J.; Proietti, M.G. Soft X-Ray Absorption Spectroscopy (Mn $L_{2,3}$ and O K) in Mixed Valence Manganites. *Surf. Rev. Let.* **2002**, *9*, 1071–1078.
12. Kanamori, H.; Yoshioka, T.; Hirose, K.; Yamamoto, T. Determination of valence state of Mn ions in $Pr_{1-x}A_xMnO_{3-\delta}$ (A = Ca, Sr) by Mn-L_3 X-ray absorption near-edge structure analysis. *J. Electron. Spectrosc.* **2012**, *185*, 129–132.
13. Abbate, M.; de Groot, F.M.F.; Fuggle, J.C.; Fujimori, A.; Strebel, O.; Lopez, F.; Domke, M.; Kaindl, G.; Sawatzky, G.A.; Takano, M.; *et al.* Controlled-valence properties of $La_{1-x}Sr_xFeO_3$ and $La_{1-x}Sr_xMnO_3$ studied by soft-X-ray absorption spectroscopy. *Phys. Rev. B* **1992**, *46*, 4511–4519.
14. Liu, R.S.; Wu, J.B.; Chang, C.Y.; Lin, J.G.; Huang, C.Y.; Chen, J.M.; Liu, R.G. Determination of Mn Valence from X-Ray Absorption Near Edge Structure and Study of Magnetic Behavior in Hole-Doped $(Nd_{1-x}Ca_x)MnO_3$ System. *J. Solid State Chem.* **1996**, *125*, 112–115.

15. Schmid, H.K.; Mader, W. Oxidation states of Mn and Fe in various compound oxide systems. *Micron* **2006**, *37*, 426–432.
16. Riedl, T.; Gemming, T.; Gruner, W.; Acker, J.; Wetzig, K. Determination of manganese valency in $La_{1-x}Sr_xMnO_3$ using ELNES in the (S)TEM. *Micron* **2007**, *38*, 224–230.
17. De Groot, F.M.F.; Grioni, M.; Fuggle, J.C.; Ghijsen, J.; Sawatzky, G.A.; Petersen, H. Oxygen 1s X-ray-absorption edges of transition-metal oxides. *Phys. Rev. B* **1989**, *40*, 5715–5723.
18. Saucke, G.; Norpoth, J.; Jooss, C.; Su, D.; Zhu, Y. Polaron absorption for photovoltaic energy conversion in a manganite-titanate pn heterojunction. *Phys. Rev. B* **2012**, *85*, 165315.
19. Blöchl, P. (Institute for Theoretical Physics, Clausthal, Germany); Norpoth, J. (Institut für Materialphysik, Göttingen, Germany); Jooss, C. (Institut für Materialphysik, Göttingen, Germany). First-Principles Study of $Pr_{1-x}Ca_xMnO_3$ with a Local Hybrid Functional. the authors' affiliation, unpublished work, 2014.
20. Jung, J.H.; Kim, K.H.; Eom, D.J.; Noh, T.W.; Choi, E.J.; Yu, J.; Kwon, Y.S.; Chung, Y. Determination of electronic band structures of $CaMnO_3$ and $LaMnO_3$ using optical-conductivity analyses. *Phys. Rev. B* **1997**, *55*, 15489–15493.
21. Mette, K.; Bergmann, A.; Tessonnier, J.-P.; Hävecker, M.; Yao, L.; Ressler, T.; Schlögl, R.; Strasser, P.; Behrens, M. Nanostructured Manganese Oxide Supported on Carbon Nanotubes for Electrocatalytic Water Splitting. *ChemCatChem* **2012**, *4*, 851–862.
22. Cressey, G.; Henderson, C.M.B.; Laan, G. Use of L-edge X-ray absorption spectroscopy to characterize multiple valence states of 3d transition metals; a new probe for mineralogical and geochemical research. *Phys. Chem. Miner.* **1993**, *20*, 111–119.
23. Alonso, J.M.; Cortés-Gil, R.; Ruiz-González, L.; González-Calbet, J.M.; Hernando, A.; Vallet-Regí, M.; Dávila, M.E.; Asensio, M.C. Influence of the Synthetic Pathway on the Properties of Oxygen-Deficient Manganese-Related Perovskites. *Eur. J. Inorg. Chem.* **2007**, *2007*, 3350–3355.
24. Gilbert, B.; Frazer, B.H.; Belz, A.; Conrad, P.G.; Nealson, K.H.; Haskel, D.; Lang, J.C.; Srajer, G.; de Stasio, G. Multiple Scattering Calculations of Bonding and X-ray Absorption Spectroscopy of Manganese Oxides. *J. Phys. Chem. A* **2003**, *107*, 2839–2847.
25. Cramer, S.P.; de Groot, F.M.F.; Ma, Y.; Chen, C.T.; Sette, F.; Kipke, C.A.; Eichhorn, D.M.; Chan, M.K.; Armstrong, W.H. Ligand field strengths and oxidation states from manganese L-edge spectroscopy. *J. Am. Chem. Soc.* **1991**, *113*, 7937–7940.
26. Frazer, B.H.; Gilbert, B.; Sonderegger, B.R.; de Stasio, G. The probing depth of total electron yield in the sub-keV range: TEY-XAS and X-PEEM. *Surf. Sci.* **2003**, *537*, 161–167.
27. Montenegro, M.J.; Lippert, T.; Müller, S.; Weidenkaff, A.; Willmott, P.R.; Wokaun, A. Pulsed laser deposition of electrochemically active perovskite films. *Appl. Surf. Sci.* **2002**, *197–198*, 505–511.
28. Montenegro, M.J.; Döbeli, M.; Lippert, T.; Müller, S.; Schnyder, B.; Weidenkaff, A.; Willmott, P.R.; Wokaun, A. Pulsed laser deposition of $La_{0.6}Ca_{0.4}CoO_3$ (LCCO) films. A promising metal-oxide catalyst for air based batteries. *Phys. Chem. Chem. Phys.* **2002**, *4*, 2799–2805.
29. Niu, J.; Deng, J.; Liu, W.; Zhang, L.; Wang, G.; Dai, H.; He, H.; Zi, X. Nanosized perovskite-type oxides $La_{1-x}Sr_xMO_{3-\delta}$ (M = Co, Mn; x = 0, 0.4) for the catalytic removal of ethylacetate. *Catal. Today* **2007**, *126*, 420–429.

30. Zhang-Steenwinkel, Y.; Beckers, J.; Bliek, A. Surface properties and catalytic performance in CO oxidation of cerium substituted lanthanum-manganese oxides. *Appl. Catal. A* **2002**, *235*, 79–92.
31. Choi, J.; Zhang, J.; Liou, S.-H.; Dowben, P.A.; Plummer, E.W. Surfaces of the perovskite manganites $La_{1-x}Ca_xMnO_3$. *Phys. Rev. B* **1999**, *59*, 13453–13459.
32. Dupin, J.-C.; Gonbeau, D.; Vinatier, P.; Levasseur, A. Systematic XPS studies of metal oxides, hydroxides and peroxides. *Phys. Chem. Chem. Phys.* **2000**, *2*, 1319–1324.
33. Fierro, J.L.G.; Tejuca, L.G. Non-stoichiometric surface behaviour of $LaMO_3$ oxides as evidenced by XPS. *Appl. Surf. Sci.* **1987**, *27*, 453–457.
34. Somorjai, G.A.; Li, Y. *Introduction to Surface Chemistry and Catalysis*; Wiley: New York, NY, USA, 1994; p. 383.
35. Jirák, Z.; Krupička, S.; Šimša, Z.; Dlouhá, M.; Vratislav, S. Neutron diffraction study of $Pr_{1-x}Ca_xMnO_3$ perovskites. *J. Magn. Magn. Mater.* **1985**, *53*, 153–166.
36. Knop-Gericke, A.; Kleimenov, E.; Hävecker, M.; Blume, R.; Teschner, D.; Zafeiratos, S.; Schlögl, R.; Bukhtiyarov, V.I.; Kaichev, V.V.; Prosvirin, I.P.; *et al.* Chapter 4 X-ray Photoelectron Spectroscopy for Investigation of Heterogeneous Catalytic Processes. *Adv. Catal.* **2009**, *52*, 213–272.
37. Follath, R.; Senf, F.; Gudat, W. Plane-grating monochromator at BESSY II using collimated light. *J. Synchrotron Rad.* **1998**, *5*, 769–771.
38. Shirley, D.A. High-Resolution X-ray Photoemission Spectrum of the Valence Bands of Gold. *Phys. Rev. B* **1972**, *5*, 4709–4714.